Engineering and Technology Journal
Journal homepage: https://etj.uotechnology.edu.iq

Effect of MXene Ti_3C_2 on the PVDF ultrafiltration membrane properties and performance

Tamara W. Abood[a*], Kadium M. Shabeeb[a], Aseel B. Alzubaydi[a], Qusay F. Alsalhy[b], Pei S. Goh[c], Ahmad F. Ismail[c], Adel Zrelli[d]

[a] Materials Engineering Dept., University of Technology-Iraq, Alsina'a street, 10066 Baghdad, Iraq.
[b] Membrane Technology Research Unit, Chemical Engineering Dept., University of Technology-Iraq, Alsina'a street, 10066 Baghdad, Iraq.
[C] Faculty of Petroleum & Renewable Energy Engineering Dept., University Technology-Malaysia, 81310, Skudai, Johor, Malaysia.
[d] Industrial and Process Chemistry Higher Institute of Applied Science and Technology Dept., Tunisia University of Gabes, Omar Ibn. ElKhattab St. 6029 Gabes, Tunisia.
*Corresponding author Email: tamara.w.abbood@uotechnology.edu.iq

HIGHLIGHTS

- MXene was initially synthesized from a MAX Phase Ti_3AlC_2 substrate through delamination
- The physical properties of the fabricated UF mixed matrix membranes with MXene were highly developed
- MXene's inclusion in PVDF solution creates a UF membrane with new self-cleaning capabilities
- MXene Ti_3C_2 enhances membranes antifouling and water permeability

ARTICLE INFO

Handling editor: Mustafa H. Al-Furaiji

Keywords:
MXene ($Ti_3C_2T_x$)
Polyvinylidene Fluoride
Hydrophilicity
Ultrafiltration Membrane
Antifouling

ABSTRACT

The problem of membrane fouling remains a significant concern in ultrafiltration, a commonly employed method in water treatment due to its high efficacy and minimal energy consumption. This study made a nanocomposite ultrafiltration membrane out of MXene Ti_3C_2 nanosheets, a new two-dimensional material, to improve the antifouling properties of PVDF membranes. It was possible to incorporate the nanosheets into the membrane structure through in situ embedment during the phase inversion process. To learn more about them, the study investigated the membranes using FESEM, FTIR, water contact angle (CA), and porosity measurements. The application of common flux and rejection tests assessed the manufactured membranes' performance. Adding MXene Ti_3C_2 to membranes made them less hydrophobic than the original membrane that wasn't mixed with anything else. The porosity and pore size of the membrane exhibit an increase in the MXene ratio. The mixed matrix membrane containing 0.5 wt% of Ti_3C_2 (M3) exhibited the lowest contact angle (CA). The modification of membrane characteristics has a positive impact on their overall performance. The membrane exhibiting the greatest porosity, specifically 0.5 wt% of Ti_3C_2, N5, demonstrated the highest flux rates for pure water and protein solution, measuring 538 L/m^2.h and 467.8 L/m^2.h, respectively. The membrane with the highest hydrophilicity, which was labeled as M3, had much better protein rejection and flux recovery rates than the pure membrane. Specifically, the recorded values for M3 were 96.6, whereas the corresponding values for the pristine membrane were 59.6. MXene Ti_3C_2 has some interesting properties, such as better water permeability, protein rejection, and excellent antifouling abilities, which makes it a possible material for changing antifouling membranes.

1. Introduction

Pressure-driven membrane filtration methods, including microfiltration (MF), ultrafiltration (UF), nanofiltration (NF), and reverse osmosis (RO), have emerged as very favorable techniques for producing clean water. These processes have garnered considerable interest from researchers in recent decades [1-5]. Many large-scale water treatment plants use membrane technologies for water treatment due to their significant benefits, such as reduced energy costs and simplified operation [6]. Nevertheless, fouling is a persistent problem in membranes, resulting in the reduction of membrane lifespan and the escalation of operational expenses [7,8]. The most recent research has focused on enhancing hydrophilic membranes made of

http://doi.org/10.30684/etj.2024.145778.1663
Received 3 January 2024; Received in revised form 19 February 2024; Accepted 19 February 2024; Available online 16 April 2024
2412-0758/University of Technology-Iraq, Baghdad, Iraq

nanocomposites for sustainable water treatment. The main goals are to enhance their resistance to fouling and to overcome the trade-off between rejecting unwanted substances and allowing water to pass through [9].

Polyvinylidene fluoride (PVDF) is a commonly used polymer in fabricating ultrafiltration (UF) membranes due to its excellent chemical resistance, mechanical strength, and thermal stability. Combined with MXene materials in a composite UF membrane, it can lead to a synergistic effect, combining the advantages of both materials [10-17].

Metal carbides known as MXenes form from MAX phases (Mn+1AXn), where n can be 1, 2, or 3, and M represents an early transition metal element. A denotes non-metallic elements from groups IV-A or III-A in MXenes. Etching removes the A element sheets from these phases [17-19]. The Tx surfaces, which are exceedingly hydrophilic and reactive, ultimately endcap MXenes; T represents O, OH, and/or F groups. To eliminate heavy metals, ions, dyes, and proteins, among other substances, $Ti_3C_2T_x$ has been the subject of the most research among MXenes utilized in water treatment and environmental sanitation [20]. MXenes have garnered significant interest owing to their unique characteristics, which include robust mechanical resilience, favorable thermal and chemical stability, a substantial surface area, effective antifouling properties, a high hydrophilic nature (allowing for easy solubility in water), metallic electronic conductivity, and the ability to form films [21]. Our group made the first lamellar MXene membrane on PVDF using a vacuum-assisted filtration method to eliminate multivalent cations from water [22]. Adding MXene ($Ti_3C_2T_x$) particles to polymers makes it possible to make films that can be used for more than one thing. Because of its great conductivities, controlled thicknesses, electrochemical properties, and high flexibility, PVDF improves the mechanical strength of the composite membrane [23]. MXenes don't get clogged up easily, are very selective for charged metals and pigments with different diameters, and can handle cations whose radiation radii are bigger than the interlayer spacing. By virtue of its exceptional mechanical properties, MXene reinforces the membrane, thereby increasing its resistance to physical stresses and prolonging its operational life. The distinctive characteristics of MXene materials can potentially augment the membrane's filtration capabilities. Potential benefits may include enhanced permeability, selectivity, and resistance to contamination. Additionally, the two-dimensional configuration of MXenes may facilitate the development of a more porous membrane structure, which may increase flux. In addition to the chemical resistance that PVDF is renowned for, MXene materials also offer chemical stability. The structural integrity and efficacy of the composite membrane will probably remain unaffected by exposure to a diverse range of chemical environments [19-23].

As a result, studies have concentrated on creating mixed-matrix MXene composite membranes using other polymeric matrices (such as PES, PVA, and PVDF) to address the limitations of pure MXenes, such as membrane swelling and reduced durability [24-28]. By inverting the phase of MXene-CA and then cross-linking it with formaldehyde, we made nanoporous mixed-matrix membranes [18]. Our group studied the effects of chemical cross-linking and the addition of MXene on membrane efficiency. We specifically investigated the impact of these factors on permeation flow and rejection compared to uncrosslinked membranes. The findings verified that membranes cross-linked by chemical means, with a 10% loading of MXene (CCAM-10%), had a substantial clean water flow rate of around 256.9 liters per square meter per hour (LMH), a water absorption capacity that exceeded 123.3% of their weight, and a porosity level of 69.7%. Additionally, these membranes displayed rejection rates of over 92.0% for rhodamine B (RhB) and over 98.0% for methyl green (MG) [18]. However, researchers conducted these studies using a stirred dead-end (DE) filtering configuration. The primary drawback of DE filtering often arises from concentration polarization and fouling resulting from the perpendicular flow of the feed stream.

In this study, mixed matrix filtration membranes consisting of MXene (Ti_3C_2) and PVDF were produced and evaluated for their flux, fouling resistance, and separation efficiency. This study also presents the impact of MXene loading in the PVDF matrix on the performance of the UF membrane. The application of ultrafiltration (UF) in membrane processes is commonly observed. The data obtained from UF filtration studies provides suitable measurements of flux and rejection capabilities.

2. Materials and methods

2.1 Materials

The membrane matrix was prepared using polyvinylidene fluoride (PVDF) with a purity of 99.5%, a molecular weight of 200,000 Mw, and sourced from Jiangsu Frechem Co., Ltd. in China. Polyvinylpyrrolidone (PVP, k30) was purchased from Sinopharm Co., Ltd., China. The NMP (N-methyl-2-pyrrolidone, 99.9%) was supplied by Hebei Shengyuan Jinlong lmp. & EXP Co., Ltd., China. The MAX phase, namely titanium aluminum carbide (Ti_3ALC_2) nanosheet with a purity of 99.95%, was acquired from Nanjing Aocheng Chemical Co., Ltd. in China. The compound NH4HF2, known as ammonium hydrogen difluoride, was provided by VWR International Co. Bovine serum albumin with MW=66.5 KDa (BSA, λmax=278 nm) was purchased from HiMedia Laboratories Pvt. Ltd.

2.2 Synthesize Ti_3C_2 MXene

Delamination approaching the MAX Phase synthesized Ti_3C_2 MXene. NH_4HF_2 in 1 M was placed in a 100-ml conical flask. Thus, 1 g of Ti_3AlC_2 MAX Phase was gradually added to NH_4HF_2. A mixture was stirred for 12 hours at 50 rpm and kept at 60°. Hydrothermal treatment followed. TiO_2 was found in MXene Nano sheets after hydrothermal treatment. The suspension solution was centrifuged and ultra-sonicated for 15 minutes to yield MXene Nano sheets and disperse powder agglomerations. The MXene mixture was then washed with ethanol and distilled water. The pieces were oven-dried at 80 ℃ for 12 hours [29].

2.3 Membranes preparation

Phase inversion technique was employed to fabricate the asymmetric UF membranes, introducing varying quantities of MXene nanosheets into the casting solution. Carefully mixing 20% PVDF powder, 2% PVP powder and 78% N-methyl-2-pyrrolidone created polymeric solutions. This mixture was stirred for 24 hours. As shown in Table 1, Ti_3C_2 MXene ratios were added and stirred for 24 hours. The solution was sonicated for an hour. Doctor-blade knives were used to cast the solution on glass plates. The membrane was soaked in a distilled water coagulation bath. The membrane was preserved in distilled water, and water changes every two days. The membranes were then immersed in 99% propanol alcohol for two days. Glycerol immersion further treated these membranes. Air-drying the membranes was the final step to store them for analysis [29].

Table 1: Casting solutions for the modified and unmodified membranes in the Ti_3C_2 MXene nanocomposite membranes case

Membranes Code	Composition			
	PVDF (wt.%)	PVP (wt.%)	NMP (wt.%)	Ti3C2 MXene (wt.%)
M0	20	2	78	0
M1	20	2	77.9	0.1
M2	20	2	77.7	0.3
M3	20	2	77.7	0.5
M4	20	2	77.3	0.7
M5	20	2	77.1	0.9

2.4 Characterization of Ti_3C_2-MXene Nano Sheet and MAX Phase Ti_3ALC_2

The field emission scanning electron microscopy (FE-SEM) technique examined the morphology of MAX phase Ti_3ALC_2 and TiO_2-MXene nanosheet materials. The FE-SEM instrument employed for the analysis was the FEI examine F50, made in Japan.

2.5 Characterization of PVDF/(Ti_3C_2) MXene Nanocomposite Membranes

The produced membranes were morphologically examined using the TESCAN-VEGA3SB FE-SEM equipment, which was supplied by EO, Elektronen-Optik Services GmbH, in Dortmund, Germany. We cross-sectioned the membranes using liquid nitrogen. The assessment included analysis of changes in the vertical surface topography, lateral forces (particularly the friction forces between the sample and tip causing cantilever torsion, measured as the left-right signal in the photodetector), and deflection. The study examined the influence of nanosheets on membrane structure by utilizing Fourier transform infrared spectroscopy (FTIR) with a Nicolet 6700 instrument manufactured by Thermo Electrons Corp. in Madison, WI, USA [19,25].

We assessed the materials' hydrophilicity by quantifying the membranes' water contact angles. We evaluated the contact angle of the membranes using the sessile drop method. The CAM110 optical contact angle device, produced in Tainan, Taiwan, was used for the investigation. The average was calculated after evaluating each sample at a minimum of five separate sites. Sections of the samples measuring 2cm × 2cm were submerged in distilled water for 15 hours to ascertain the porosity of the membranes. We then removed the water from the damp films and collected and measured any excess droplets on the membrane surface using blotting paper. After drying in an oven for 12 hours, we measured the dry weight of the membrane. We calculated the membrane porosity using Equation (1) [26]. We subjected each membrane sample to five porosity measurements and averaged the resulting values.

$$\varepsilon\% = \frac{Ww - Wd}{A \times L \times p} \quad (1)$$

where:ε= porosity A= area of membrane (cm^2); W_w and W_d = membranes' wet and dry weights; L= thickness (cm), ρ= density of water.

Equation (2), which accounts for the membrane's porosity and the flow of clean water, was employed to estimate the average pore sizes (rm).

$$rm = \sqrt{\frac{(8\mu LQ)x(2.9-1.75\varepsilon)}{\Delta P.\varepsilon.A}} \quad (2)$$

where: rm= mean pore size μ= water viscosity, Q= collected volume of pure water flux per unit time (m^3/s), ΔP= operation pressure, L and A= thickness and effective membrane area [27].

2.6 Membrane performance

2.6.1 Pure water flux

In a custom-made dead-end apparatus, membranes of laboratory scale, as shown in Figure 1, possessing a membrane area of 13.69 cm^2, underwent testing to assess their water permeability and separation efficiency. Each membrane underwent compression at 0.2 MPa pressure for 30 minutes while also being exposed to pure water to ensure consistent flux. The water fluxes were assessed after lowering the pressure to the operational flux level of 0.1MPa. The permeate flux (J) was obtained utilizing Equation (3) [28].

$$Flux\ (J) = \frac{Collected\ permeate\ volume\ (V,m^3)}{Efficient\ membranes\ area(A,m^2)x\ time\ (t)} \quad (3)$$

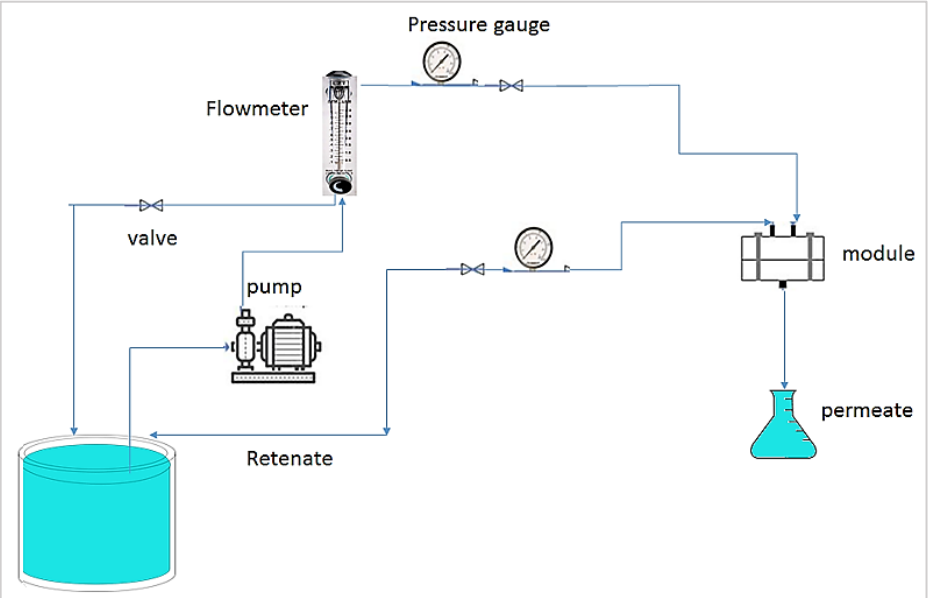

Figure 1: Schematic diagram illustrating the cross-flow filtration system

After that, bovine serum albumin (BSA) solution with a concentration of 1000 mg/L was utilized to evaluate the membrane rejection (R) using Equation 4 [28]:

$$R(\%) = \frac{Cf-Cp}{Cf} \times 100\% \quad (4)$$

where *Cp* and *Cf* are the BSA concentrations in the permeate and feed solutions, respectively.

2.6.2 Antifouling assessment

We used the solution depletion approach to assess the static protein adsorption onto membranes. BSA served as a prototype foulant. The membranes, measuring 13.69 cm^2, were produced and then submerged in a 1 g/L BSA solution in phosphate-buffered saline (PBS, pH 7.4) at 25 ℃ for 20 hours. Using the created calibration curve, an ultraviolet spectrophotometer operating at 280 nm detected the concentration difference prior to and following adsorption. The variation indicates each membrane's adsorption capability. After conducting tests for water permeability and separation performance, we cleaned the protein-fouling membranes in pure water for 15 minutes. The water flow was then measured once more in terms of Jw L/m^2.h. As shown in [29], we computed the flux recovery ratio (FRR) using the following equation:

$$FRR = \frac{Jw,2}{Jw,1} \times 100\% \quad (5)$$

where 1 and 2 denote the flux before and after cleaning.

The following equations [28,29] can be used to analyze the fouling process more precisely by incorporating the total fouling ratio (Rt) along with the reversible and irreversible fouling ratios (Rr and Rir):

$$Rt(\%) = \left[1 - \frac{Jp}{Jw,1}\right] \times 100 \quad (6)$$

$$Rr(\%) = \left[\frac{Jw,2-Jp}{Jw,1}\right] \times 100 \quad (7)$$

$$Rir(\%) = \left[\frac{Jw,1-Jw,2}{Jw,1}\right] \times 100 \quad (8)$$

3. Results and discussion

3.1 Ti_3C_2 Analysis

Figure 2a showed FESEM images of MAX phase Ti_3ALC_2 and Figure 2b showed FESEM images of Ti_3C_2 MXene nanosheets. It found that MAX phase Ti_3ALC_2 and Ti_3C_2 MXene displayed a classical 2D structure. In contrast, the cross-sectional FESEM image of Ti_3C_2, which is illustrated in Figure 2b, suggests that the accordion-like Ti_3C_2 nanosheets keep stacked after etching of Ti_3AlC_2, and the inter-lamellar spacing between Ti_3C_2 nanosheets.

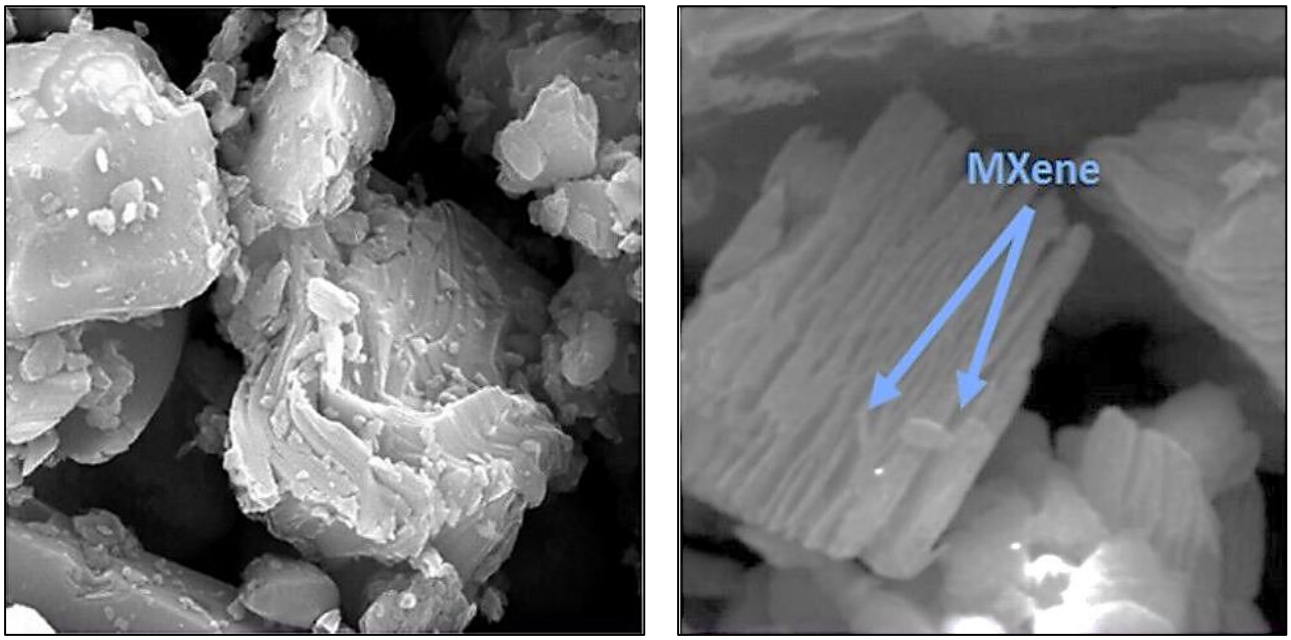

(a) **(b)**

Figure 2: a) Shows FESEM images Max phases Ti_3ALC_2 Nano sheets b) Shows FESEM images Ti_3C_2 MXene nano sheet

3.2 Nanocomposite membrane characterization

3.2.1 Field emission scanning electron microscopy for nanocomposite membranes

In Figures 3 and 4, PVDF membranes have an asymmetric structure with a compact top layer and a porous sub-layer with a spongy and finger-like shape. The structural features of the blended and bare PVDF membranes are similar, demonstrating that Ti_3C_2 inclusion during phase inversion did not affect membrane development. Water separation is better with the membrane's spongy, dense lower layer. Macrovoids in membranes may reduce their long-term stability [30,31]. Hydrophilic functional groups in MXene undergo accelerated phase inversion. The polymer matrix became more attracted to the non-solvent medium during coagulation. Enhancing the membrane with a thin, compact skin layer sped up the process [32]. While the sub-layer preserves membrane mechanical integrity, this upper layer is crucial to solution penetration and separation [33]. All membranes created have an asymmetric structure with a finger-like top layer of dense material and a lower layer of porous material, demonstrating that these nanosheets did not impair membrane creation. M3's thin skin layer may explain its high water permeability.

Figure 5 provides additional evidence to support the characterization of the PVDF membrane surface using FTIR analysis. The PVDF membrane, in its native state, exhibits a significant peak at 1402 cm^{-1}, which corresponds to the stretching vibration of carbon-hydrogen (C-H) bonds. Furthermore, the spectroscopic analysis reveals the presence of two distinct bands at wavenumbers of 1275 cm^{-1} and 1178 cm^{-1}, which can be ascribed to the vibrational modes associated with the C-F bonds. The incorporation of MXene into the virgin PVDF membrane led to a discernible attenuation in the asymmetrical and symmetrical stretching of C-F bonds (1178 cm^{-1} and 1275 cm^{-1}, respectively), as well as the vibration of the C-H bond (1042 cm^{-1}) in comparison to the initial spectra. The results of the integration of Ti_3C_2 MXene nanosheets are illustrated in Figure 10. The inclusion of Ti_3C_2 MXene leads to a significant augmentation of the peak intensities seen at 1650, 2349, and 3767 cm^{-1}. The identified peaks suggest several functional groups, such as hydroxyl, methyl, and carbonyl. These peaks, which suggest the formation of pristine and nanocomposite membranes, have been discovered in recent experiments [34,35]. The spectral analysis results on the membrane revealed that introducing Ti_3C_2 MXene nanosheet did not induce any alterations in the vibrational bands' properties. This implies that no alterations were observed in either the chemical composition of the membrane or its non-covalent interaction with Ti_3C_2 MXene.

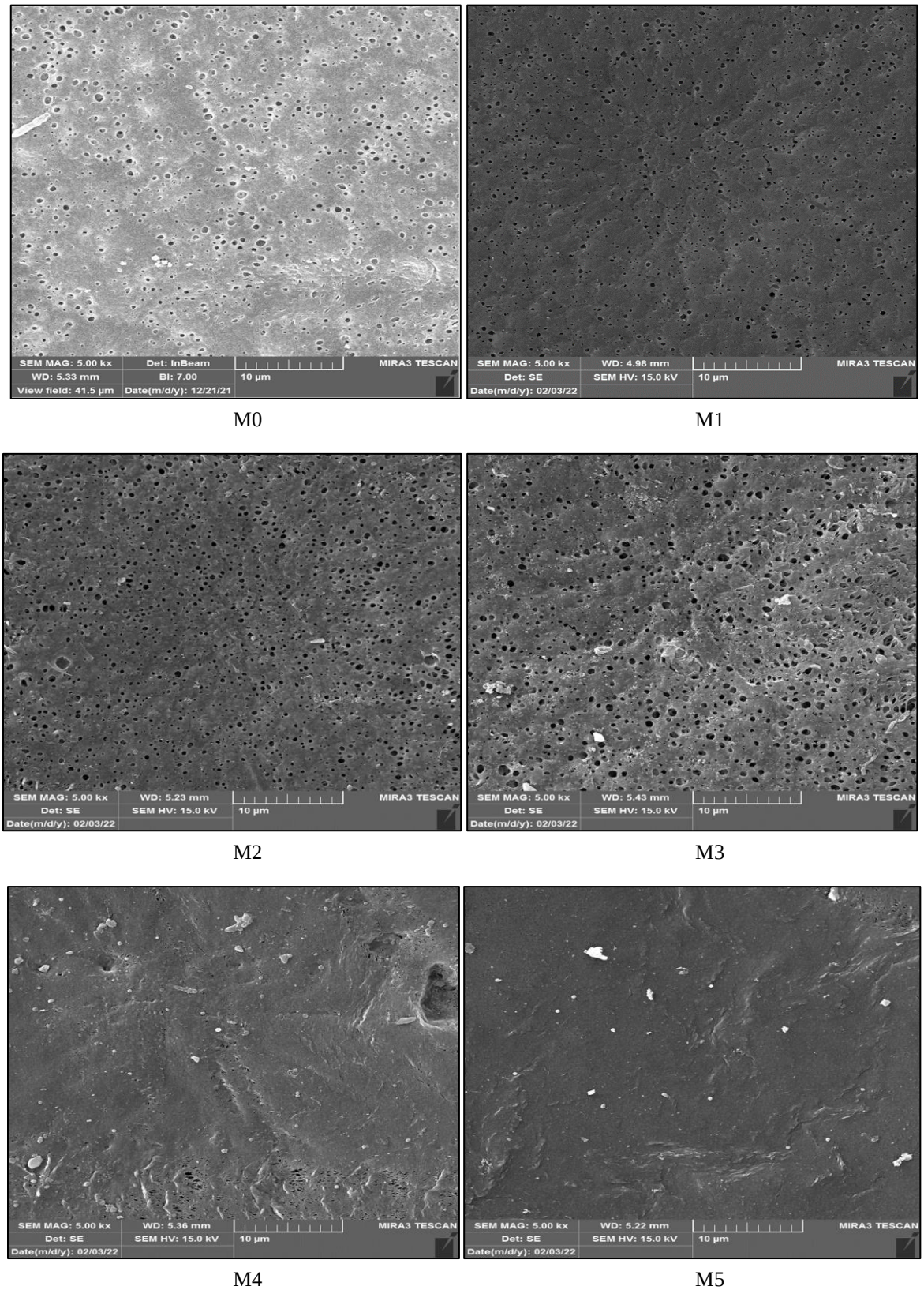

Figure 3: Surface images of the fabricated PVDF/Ti_3C_2 MXene membranes

Hydrophilicity is a basic property of filtration membranes, which increases fouling resistance. The neat PVDF membrane had a 64.57° contact angle. After the Ti_3C_2 MXene modification, its value dropped slowly. The contact angles of nanocomposite membranes with 0.1–0.5 g dropped from 55.2° to 38.5° after adding nanosheets, as shown in Figure 6. The best contact angles were 38.5° and 39.5° for 0.4 g and 0.5 g nanosheet loadings, respectively. Similar to reference [36–39], the results suggested that hydrophilic nanosheet migration of membrane surfaces during phase inversion reduced interfacial energy and increased hydrophilicity. However, adding nanosheets increased contact angles again. Nanosheet aggregation at the

surface under high loading conditions likely generated a non-homogeneous membrane structure or leaching. Figure 6 shows that the findings matched [40].

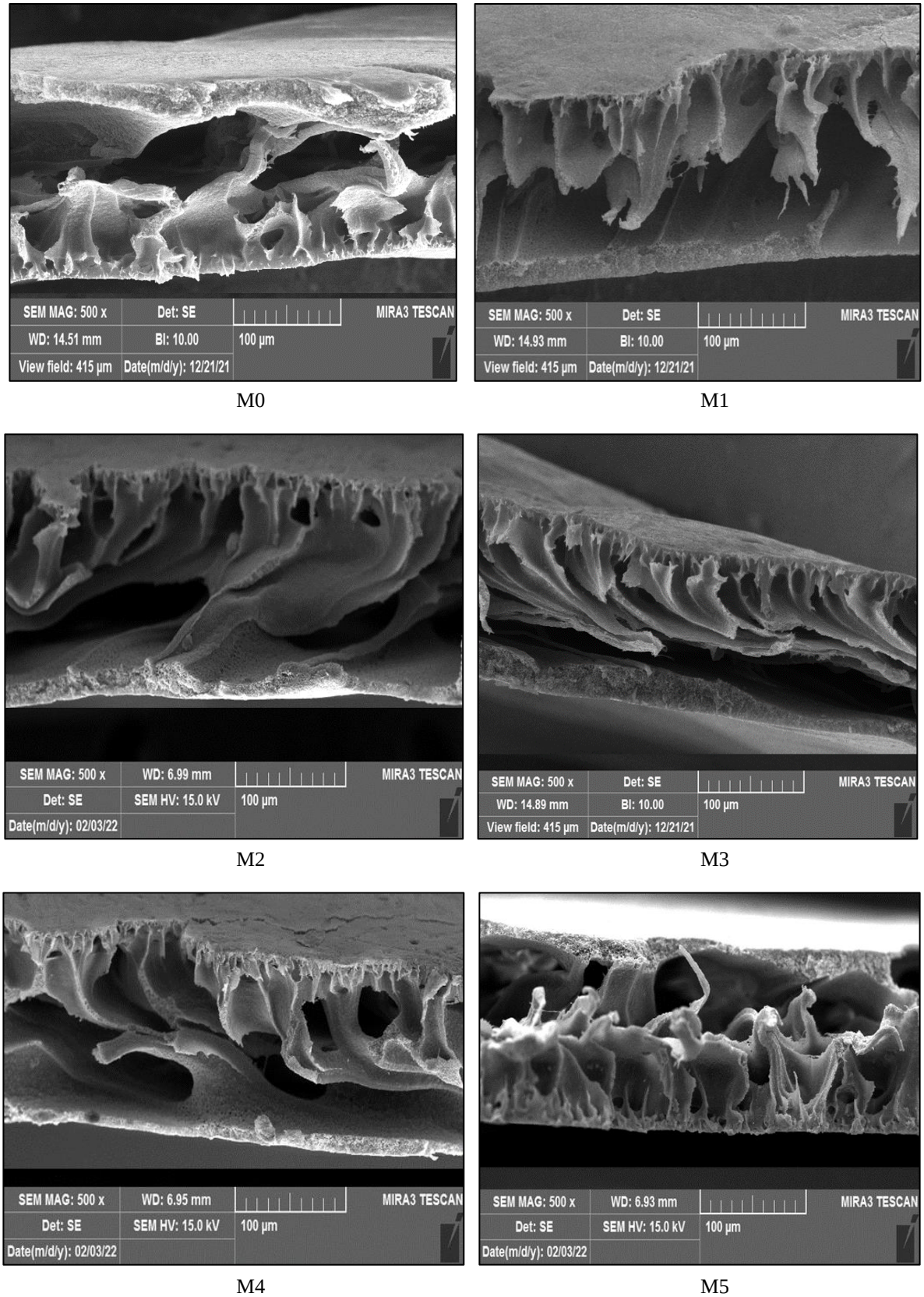

Figure 4: Cross-section images of the fabricated PVDF/Ti_3C_2 MXene membranes

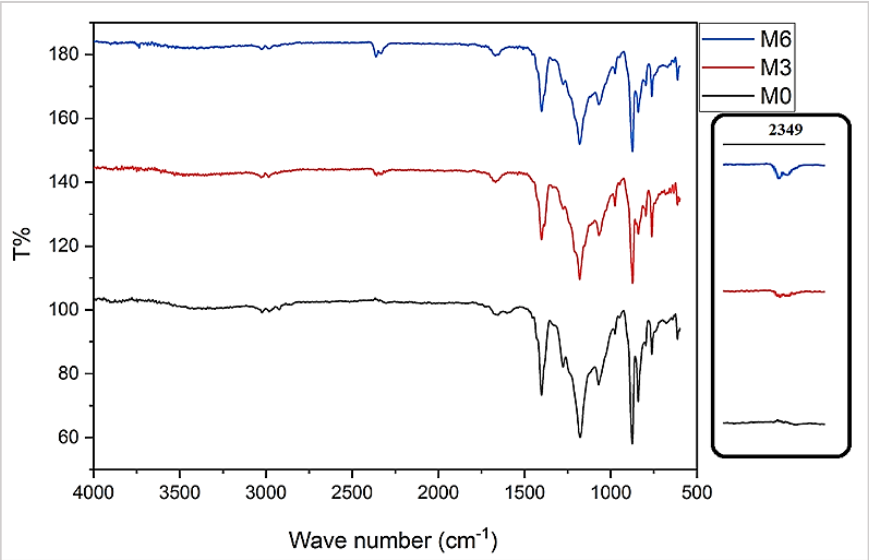

Figure 5: FTIR spectra for modified and unmodified PVDF/Ti_3C_2 membranes

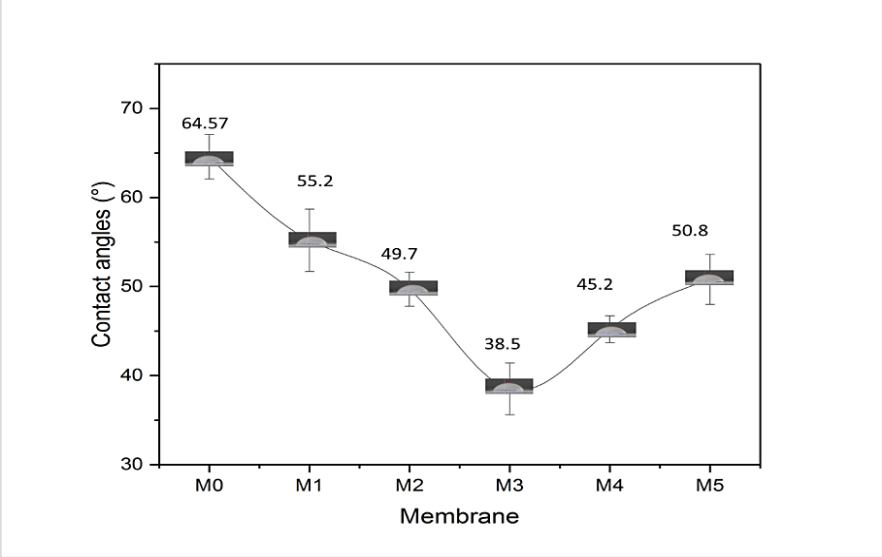

Figure 6: Contact angle of PVDF/Ti_3C_2 MXene membranes

The distribution range and mean pore size (nm) of each membrane have also been determined using the FESEM image, and the results are shown in Figure 7. Among the several nanocomposite membranes, the unmodified (PVDF) membrane had the largest mean pore size (30.37 nm) and pore size distribution (0-80 nm). The results showed that adding 0.1 g of (MXene) Nano sheet caused certain structural alterations that resulted in a surge in the mean pore size (394.6 nm) and a significantly wider pore dispersion (200-600 nm). As the quantity of nanosheets increases, there has been a consistent increase in the average pore size and the magnitudes of their distribution. Figure 7. At 0.5 g of nanoadditives, the membrane of the nanocomposites, aside from the tidier distribution (200–1200 nm), has the largest pore size (627 nm). The distribution and mean pore size gradually decreased, and this decrease was proportionate to each increase in the ratio of nano additives in the membrane matrix. The filling of PVDF matrix pores by nanosheets can account for the decrease in mean pore size.

The mean pore size seen in PVDF/Ti_3C_2 MXene mixed matrix membranes (MMMs) at different nanoparticle concentrations is shown in Figure 8. The membranes generated at a concentration of 0.5 wt% exhibit an increase in both the maximum porosity and mean pore. They think the effect they saw happened because more Ti_3C_2 MXene was added to the Ti_3C_2 MXene nanosheet mixed matrix membranes (MMMs), making them more hydrophilic. This, in turn, promotes a higher rate of solvent-solvent exchange during the coagulation process, resulting in an increased frequency of pore radius and higher pore density [41,42]. The obtained results validate the data presented in the FESEM image of the top surface.

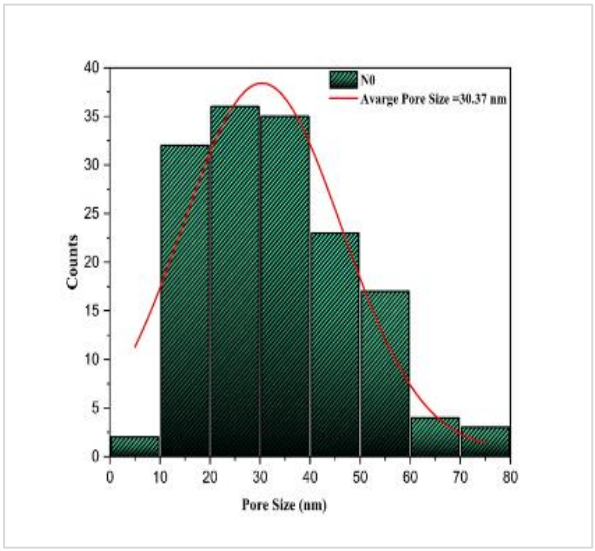

M0

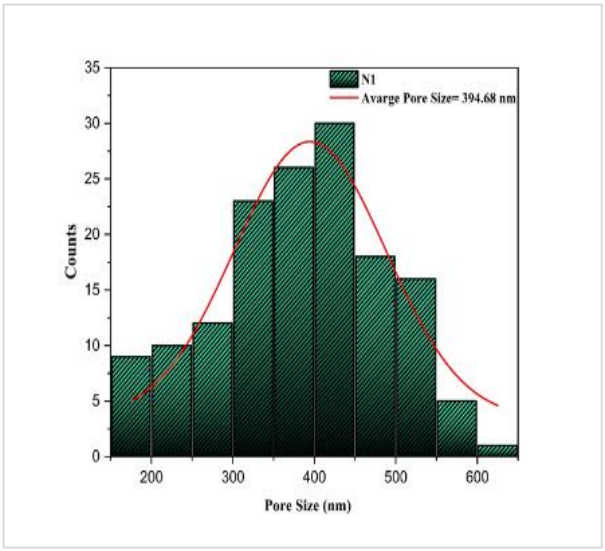

M1

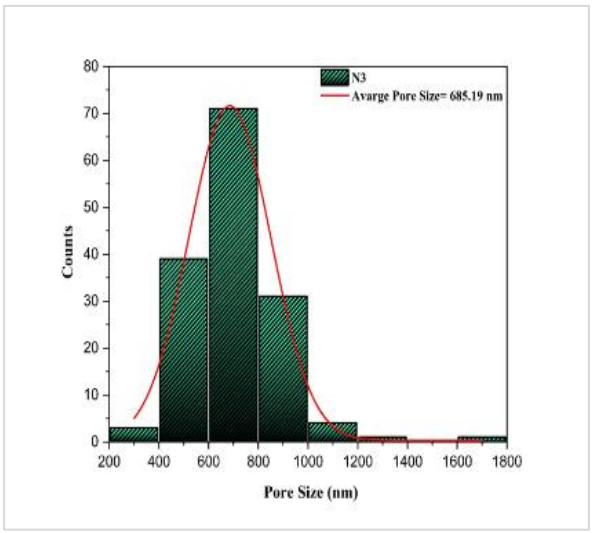

M2

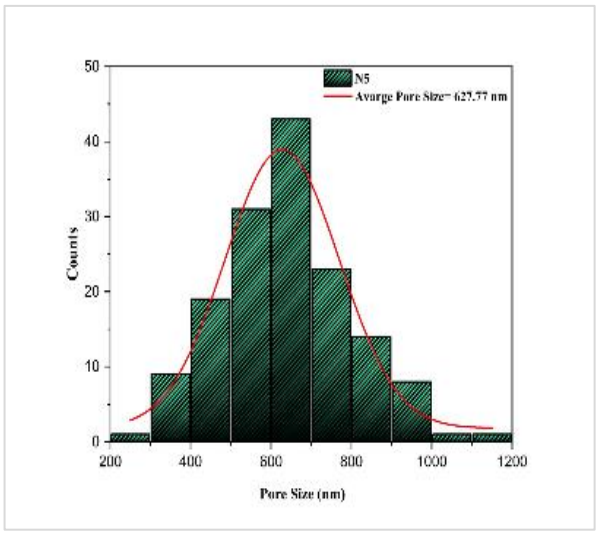

M3

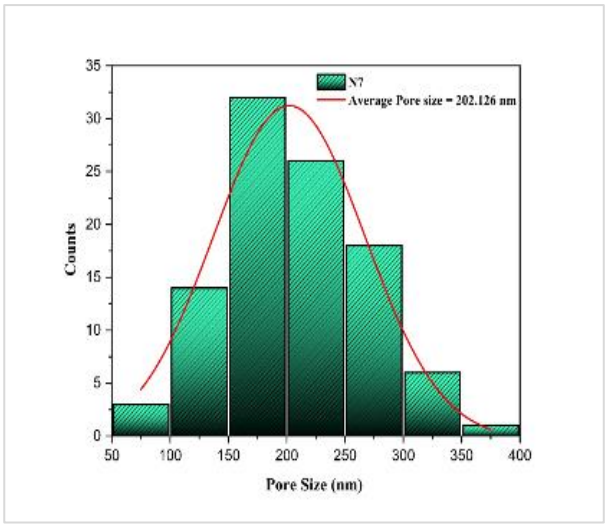

M4

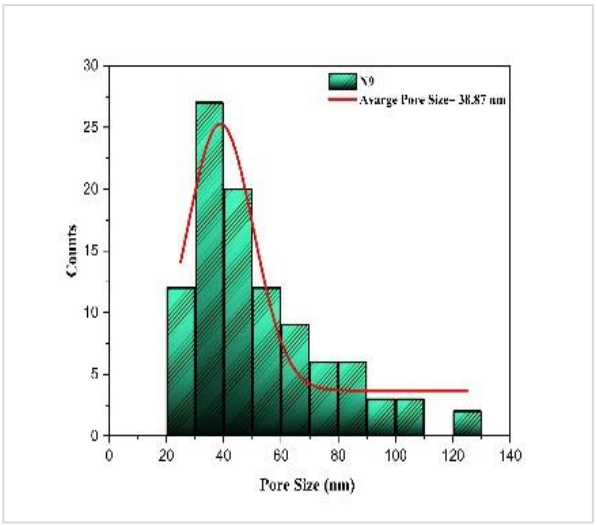

M5

Figure 7: Pore size distribution of the membranes prepared at various MXene nanosheets content

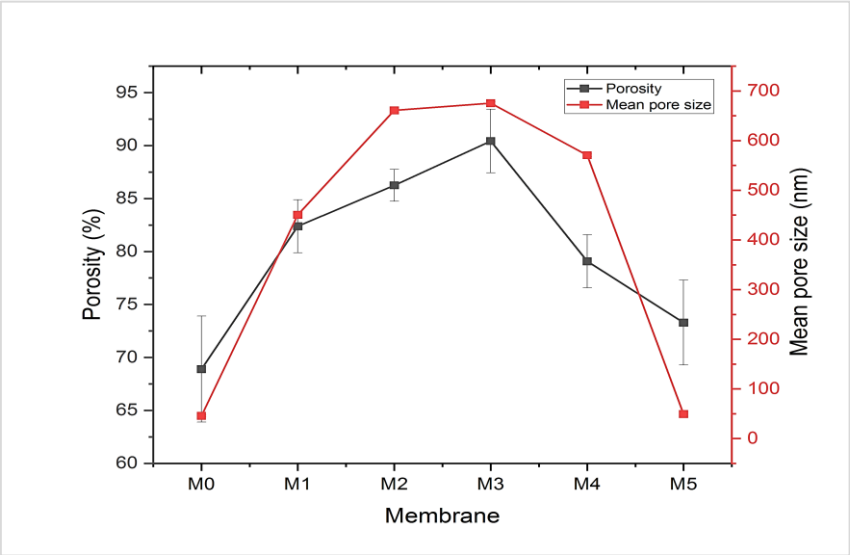

Figure 8: PVDF/Ti_3C_2 membranes porosity and mean pore size

Calculated at 0.1 MPa, pure water flux (PWF) Figure 9a shows how Mxene Ti_3C_2 content affects PVDF/MTCF membrane performance. The PVDF/Mxene Ti_3C_2 composite membrane's pure water flux rose dramatically with Mxene Ti_3C_2 up to 0.5 wt%, but greater concentrations may cause pore blockage and decrease pure water flux [43]. Figure 9b shows that the BSA solution decreased permeation flux somewhat. Solutes on the membrane surface and in the pores contaminate the membrane and reduce filtration flow [45]. Membrane fouling is unavoidable; however, using a hydrophilic substance inside the membrane helps reduce it. In this study, Mxene Ti_3C_2 increased membrane hydrophilicity and reduced contamination. Modeling fouling using BSA assessed membrane antifouling properties. The hydrophobic characteristic of a clean PVDF membrane reduced BSA rejection to 59.6 [46]. Mxene Ti_3C_2 enhanced BSA rejection to 96.3%.

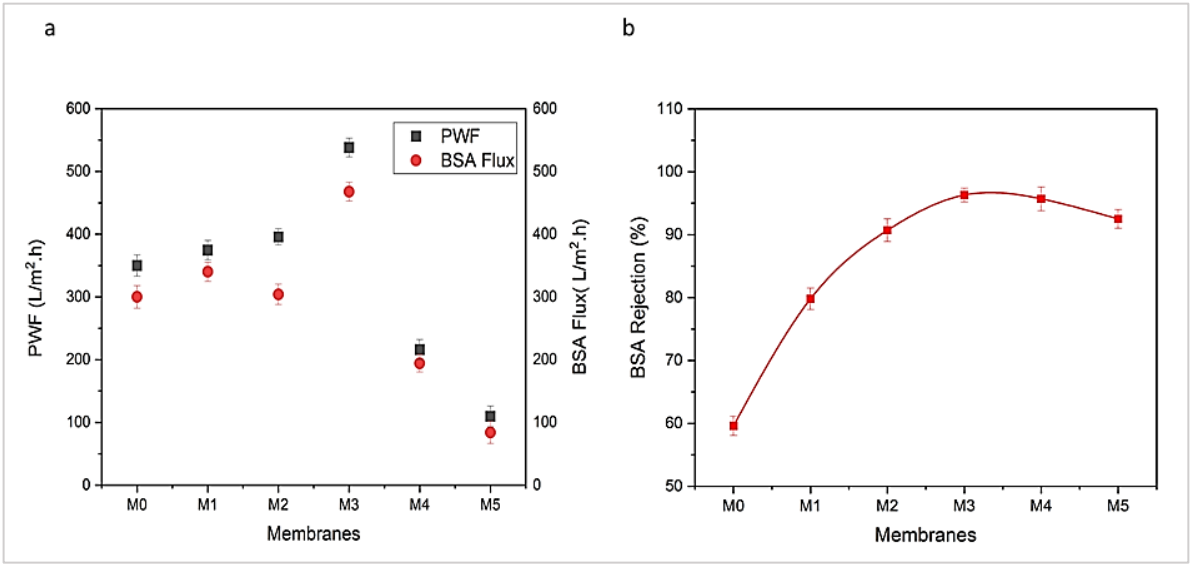

Figure 9: a**)** Pure water flux and bovine serum albumin (BSA flux of MXeneTi_3C_2/(PVDF) membranes. b) Bovine serum albumin (BSA) rejection of the neat PVDF and MXene /PVDF membrane

We calculated the flow recovery ratio (FRR) to perform a more thorough evaluation of the antifouling capabilities of the membranes. The results are shown in Figure 10. The clean PVDF membrane had the lowest FRR, at 59.3%, of all the nanocomposite membranes. The membrane M3, which has a higher hydrophilicity than the others, has the highest flux recovery ratio (89.6%). Reversible and irreversible fouling are the two types that arise from the interaction between the foulants and the membrane surface that determines this categorization. The comparatively weak contact between fouling particles and the membrane surface facilitates their simple removal and reversible fouling. Reversible fouling was discovered across most of the accumulated boundary surface area (BSA) on M3.

Displays the overall fouling ratio (Rt), the fouling ratio that can be reversed (Rr), and the fouling ratio that cannot be reversed (Rir) for all the membranes that were created. Figure 10 shows that the membrane with MXene nanosheets added to it

had a slightly higher overall fouling resistance than the PVDF membrane, which was not changed in any way. With increased MXene concentration, the membrane dramatically reduced irreversible resistance. Concurrently, the Rr value tended to have a positive correlation with the MXene content. The results showed that the nanocomposite membrane's improved hydrophilicity and reduced surface roughness facilitated the easy elimination of foulants. Consequently, the nanocomposite membrane exhibited superior antifouling characteristics compared to the clean membrane.

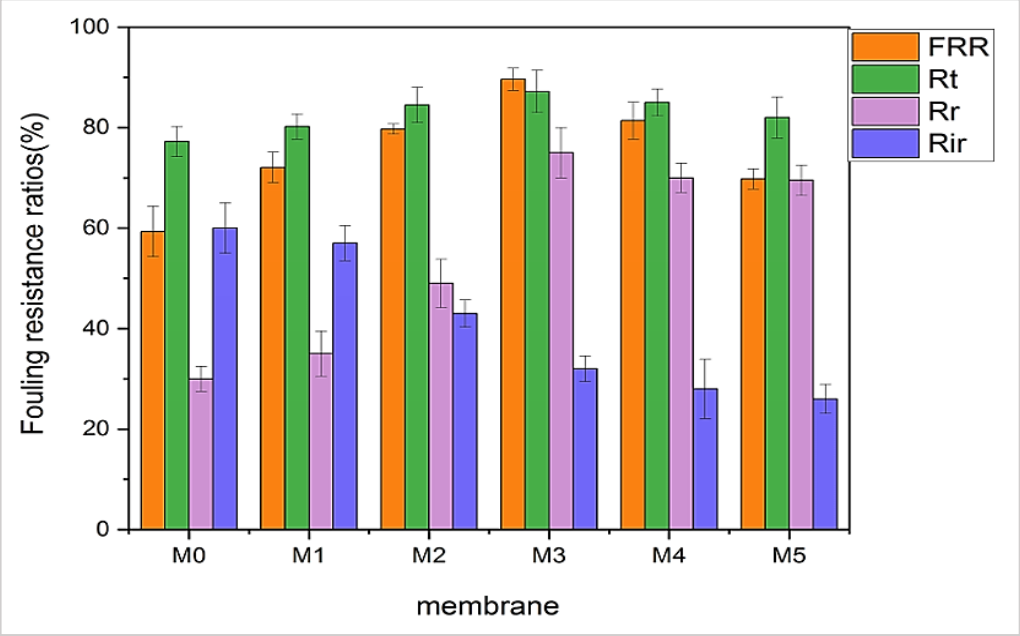

Figure 10: Fouling resistance ratios and Water flux recovery ratio of MXene Ti_3C_2/PVDF membranes

The results obtained in this work were compared with other studies on ultrafiltration membranes that incorporated different MXene nanosheets to enhance antifouling capabilities, as outlined in Table 2. The membrane containing MXene Ti_3C_2 exhibited significant improvements in both water penetration and protein rejection, which can be attributed to the improved hydrophilicity induced by the incorporation of MXene Ti_3C_2.

Table 2: Comparison of mxene membranes in terms of water penetration and protein rejection and hydrophilicity

No. sample	Polymer Concentration	Mxene ratio	Contact angle (degree)	PWF L/m^2 .h	Rejection ratio%	FRR (%)	Pollutant	Ref.
PES/ MXENE	15% PES	1	78.4	390	98	76.1	BSA	[47]
MXene-PANI/PES	19% PES	0.02	47.5	175	90	90	BSA	[48]
PES/MXene	16% PES	0.05	87	685	98	91	BSA	[49]
PES-Ni@MXene	15% PES	1	54.15	1181	98.35	64.4	BSA	[50]
PVDF/MXENE	20% PVDF	0.5	38.5	538	96.3	89.6	BSA	This work

4. Conclusion

This work synthesized fouling-resistant PVDF membranes for ultrafiltration (UF) applications using nanocomposite MXene Ti_3C_2 Nanosheets. We used a range of MXene Ti_3C_2 samples to measure the nanosheet-to-polymer ratio. Thoroughly examining and tracking the changes brought about by the additions required a variety of advanced surface and structural chemistry studies. Tests that evaluated the flow of clean water and the rejection of bovine serum albumin (BSA) were utilized to assess the efficiency of the mixed matrix membranes. The addition of Ti_3AlC_2 was found to enhance the hydrophilicity and the mean pore size. This statement pertains to the observation of irregular reversal trends in certain characteristics. The fluxes of pure water and BSA solution demonstrated this behavior in the membrane's performance. Concerning FRR and BSA rejection, M3 performed best; this may have been because of its higher hydrophilicity than the other membranes. This investigation shows promising results for applying MXene Ti_3C_2 as a possible supplement to reduce fouling in PVDF membranes. These findings call for more investigation into the created mixed matrix membrane's functionality, especially when evaluating complex matrix samples over an extended time.

Author contributions

Conceptualization, T. Abood, K. Shabeeb, A. Alzubaydi, Q. Alsalhy, P. Goh, A. Ismail and A. Zrelli; data curation, T. Abood and Q. Alsalhy; Formal analysis, T. Abood, K. Shabeeb, A. Alzubaydi, Q. Alsalhy; supervision, K. Shabeeb, A. Alzubaydi and Q. Alsalhy; Visualization, T. Abood and Q. Alsalhy; writing—original draft, K. Shabeeb, A. Alzubaydi and Q. Alsalhy; writing—review and editing, T. Abood, K. Shabeeb, A. Alzubaydi, Q. Alsalhy, P. Goh, A. Ismail and A. Zrelli;. All authors have read and agreed to the published version of the manuscript.

Funding

This research received no specific grant from any funding agency in the public, commercial, or not-for-profit sectors.

Data availability statement

The data that support the findings of this study are available on request from the corresponding author.

Conflicts of interest

The authors declare that there is no conflict of interest.

References

[1] X. Lu, S. R. Castrillón, D. L. Shaffer, J. Ma, M. Elimelech, In Situ Surface Chemical Modification of Thin-Film Composite Forward Osmosis Membranes for Enhanced Organic Fouling Resistance, Environ. Sci. Technol. https://doi.org/10.1021/es403179m

[2] B. Al-Najar, C. D. Peters, H. Albuflasa, N. P. Hankins , Pressure and osmotically driven membrane processes: A review of the benefits and production of nano-enhanced membranes for desalination, Desalination, 479 (2020) 114323. https://doi.org/10.1016/j.desal.2020.114323

[3] M. Bodzek, K. Konieczny, A. Kwiecińska, Application of membrane processes in drinking water treatment–state of art, Desalin. Water Treat., 35 (2011) 164–184. https://doi.org/10.5004/dwt.2011.2435

[4] A. Modi, J. Bellare, Zeolitic imidazolate framework-67/carboxylated graphene oxide nanosheets incorporated polyethersulfone hollow fiber membranes for removal of toxic heavy metals from contaminated water, Sep. Purif. Technol., 249 (2020) 117160. https://doi.org/10.1016/j.seppur.2020.117160

[5] H. Karimnezhad, A. H. Navarchian, T Tavakoli Gheinani., S. Zinadini, Incorporation of iron oxyhydroxide nanoparticles in polyacrylonitrile nanofiltration membrane for improving water permeability and antifouling property, React. Funct. Polym., 135 (2019) 77–93. https://doi.org/10.1016/j.reactfunctpolym.2018.12.016

[6] M. T. Tsehaye, J. Wang, J. Zhu, S. Velizarov, B. Van der Bruggen, Development and characterization of polyethersulfone-based nanofiltration membrane with stability to hydrogen peroxide, J. Membr. Sci., 550 (2018) 462–469. https://doi.org/10.1016/j.memsci.2018.01.022

[7] C. Wei, Z. He, L. Lin, Q. Cheng, K. Huang, S. Ma, L. Chen, Negatively charged polyimide nanofiltration membranes with high selectivity and performance stability by optimization of synergistic imidization, J. Membr. Sci., 563 (2018) 752–761. https://doi.org/10.1016/j.memsci.2018.06.046

[8] S.-S. Shen, H. Chen, R.-H. Wang, W. Ji, Y. Zhang, R. Bai, Preparation of antifouling cellulose acetate membranes with good hydrophilic and oleophobic surface properties, Mater. Lett., 252 (2019) 1–4. https://doi.org/10.1016/j.matlet.2019.03.089

[9] M. Safarpour, A. Khataee, V. Vatanpour, Preparation of a novel polyvinylidene fluoride (PVDF) ultrafiltration membrane modified with reduced grapheme oxide/titanium dioxide (TiO_2) nanocomposite with enhanced hydrophilicity and antifouling properties, Ind. Eng. Chem. Res.,53 (2014) 13370–13382. https://doi.org/10.1021/ie502407g

[10] T. W. Abood, K. M. Shabeeb, A. B. Alzubaydi, H. S. Majdi, R. A. Al-Juboori, Q. F. Alsalhy, Effect of MAX Phase Ti3ALC2 on the Ultrafiltration Membrane Properties and Performance, Membranes, 13 (2023). https://doi.org/10.3390/membranes13050456

[11] Q. F. Alsalhy, J. M. Ali, A. A. Abbas, A. Rashed, B. V. Bruggen, S. Balta, Enhancement of poly (phenyl sulfone) membranes with ZnO nanoparticles, Desalin. Water Treat., 51 (2013).

[12] Q. F. Alsalhy, F. H. Al-Ani, A. E. Al-Najar, S. I. Jabuk, A study of the effect of embedding ZnO-NPs on PVC membrane performance use in actual hospital wastewater treatment by membrane bioreactor, Chem. Eng. Process. Process Intensif., 130 (2018) 262-274. https://doi.org/10.1016/j.cep.2018.06.019

[13] Q. F. Alsalhy, J. M. Ali, A. A. Abbas, A. Rashed, B. V. Bruggen, B. Stefan, Enhancement of poly (phenyl sulfone) membranes with ZnO nanoparticles, Desalination and Water Treatment (2013) 1-12.

[14] M. J. Jamed, A. A. Alanezi, Q. F. Alsalhy, Effects of embedding functionalized multi-walled carbon nanotubes and alumina on the direct contact poly(vinylidene fluoride-cohexafluoropropylene) membrane distillation performance, Chem. Eng. Commun., 206 (2019) 1035-1057. https://doi.org/10.1080/00986445.2018.1542302

[15] M. M. Aljumaily, M. A. Alsaadi, N. A. Hashim, Q. F. Alsalhy, R. Das, F. S. Mjalli, Embedded high-hydrophobic CNMs prepared by CVD technique with PVDF-co-HFP membrane for application in water desalination by DCMD, Desalin. Water Treat., 142 (2019) 37–48.

[16] A. J. Sadiq, K. M. Shabeeb, B. I. Khalil, Q. F. Alsalhy, Effect of embedding MWCNT-g-GO with PVC on the performance of PVC membranes for oily wastewater treatment, Chem. Eng. Commun., 207 (2020) 733–750. https://doi.org/10.1080/00986445.2019.1618845

[17] A. J. Sadiq, E. S. Awad, K. M. Shabeeb, B. I. Khalil, S. M. Al-Jubouri, T. M. Sabirova, N. A. Tretyakova, H. S. Majdi, Q. F. Alsalhy, A. J. Braihi, Comparative study of embedded functionalized MWCNTs and GO in Ultrafiltration (UF) PVC membrane: interaction mechanisms and performance, Int. J. Environ. Anal. Chem., 103 (2020) 415-36. https://doi.org/10.1080/03067319.2020.1858073

[18] A.G. Fane, R. Wang, M. X. Hu, Synthetic membranes for water purification: status and future, Angew Chem. Int. Ed. Eng., 54 (2015) 3368-3386. https://doi.org/10.1002/anie.201409783

[19] R. Alfahel, R. S. Azzam, M. Hafiz, A. H. Hawari, R. P. Pandey, K. A. Mahmoud, M. K. Hassan, A. A. Elzatahry, Fabrication of fouling resistant $Ti_3C_2T_x$ (MXene)/cellulose acetate nanocomposite membrane for forward osmosis application, J. Water Process Eng., 38(2020) 101551. https://doi.org/10.1016/j.jwpe.2020.101551

[20] K. Rasool, R. P. Pandey, P. A. Rasheed, S. Buczek, Y. Gogotsi, K. A. Mahmoud, Water treatment and environmental remediation applications of two-dimensional metal carbides (MXenes), Mater. Today, 30 (2019) 80–102. https://doi.org/10.1016/j.mattod.2019.05.017

[21] M. Naguib, M. Kurtoglu, V. Presser, J. Lu, J. Niu, M. Heon, L. Hultman, Y. Gogotsi, M. W. Barsoum, Two-Dimensional Nanocrystals Produced by Exfoliation of Ti_3AlC_2, Adv. Mater., 23 (2011) 4248–4253. https://doi.org/10.1002/adma.201102306

[22] K. Rasool, K. Mahmoud, D. Johnson, M. Helal, G. Berdiyorov, Y. Gogotsi, Efficient Antibacterial Membrane based on Two-Dimensional Ti_3C_2Tx (MXene) Nanosheets, Sci. Rep., 7 (2017) 1598. https://doi.org/10.1038/s41598-017-01714-3

[23] Z. Ling, C. E. Ren, M.-Q. Zhao, J. Yang, J. M. Giammarco, J. Qiu, M.W. Barsoum, Y. Gogotsi, Flexible and conductive MXene films and nanocomposites with high capacitance, Proc. Natl. Acad. Sci., 111 (2014) 16676-1661. https://doi.org/10.1073/pnas.1414215111

[24] J. Li, X. Li, B. Bruggen, An MXene based membrane for molecular separation, Environ. Sci. Nano., (2020) 1289–1304. https://doi.org/10.1039/C9EN01478K

[25] R. S. Azam, Enhancing The Fouling Resistance and Rejection of Cellulose Acetate [Ca]/Mxene [Ti_3C_2Tx] Nanocomposite Membranes, Qatar University, Doha, Qatar, 2021.

[26] J. Zhu, J. Hou, Y. Zhang, M. Tian, T. He, J. Liu, V. Chen, Polymeric antimicrobial membranes enabled by nanomaterials for water treatment, J. Membr. Sci., 550 (2018) 173–197. https://doi.org/10.1016/j.memsci.2017.12.071

[27] E. H. b. Alosaimi, H. M. A. Hassan, I. H. Alsohaimi, Q. Chen, S. Melhi, A.A. Younes, W.H. El-Shwiniy, Fabrication of sulfonated polyethersulfone ultrafiltration membranes with an excellent antifouling performance by impregnating with polysulfopropyl acrylate coated ZnO nanoparticles, Environ. Technol. Innov., 25 (2022) 102210. https://doi.org/10.1016/j.eti.2021.102210

[28] S. Beisl, S. Monteiro, R. Santos, A. S. Figueiredo, M. G. Sánchez-Loredo, M. A. Lemos, F. Lemos, Minhalma M. , M. N. de Pinho, Synthesis and bactericide activity of nanofiltration composite membranes–Cellulose acetate/silver nanoparticles and cellulose acetate/silver ion exchanged zeolites, Water Res., 149 (2019) 225–231. https://doi.org/10.1016/j.watres.2018.10.096

[29] H. Wang, Y. Wu, J. Zhang, G., Li, H. Huang, X. Zhang, Q. and Jiang, Enhancement of the electrical properties of MXene Ti3C2 nanosheets by post-treatments of alkalization and calcination, Mater. Lett., 160 (2015) 537-540. https://doi.org/10.1016/j.matlet.2015.08.046

[30] M. G. García, J. Marchese, N. A. Ochoa, Effect of the particle size and particle agglomeration on composite membrane performance, J. Appl. Polym. Sci., 118 (2010) 2417–2424. https://doi.org/10.1002/app.32274

[31] J. M. Duval, A. J. B. Kemperman, B. Folkers, M. H. V. Mulder, Desgrandchamps G., Smolders C.A., Preparation of zeolite filled glassy polymer membranes, J. Appl. Polym. Sci., 54 (1994) 409–418. https://doi.org/10.1002/app.1994.070540401

[32] C. Casado-Coterillo, Mixed Matrix Membranes, Membranes, 9 (2019)149. https://doi.org/10.3390/membranes9110149

[33] H. E. Karahan, K. Goh, C. Zhang, E. Yang, C. Yıldırım, C. Y. Chuah, M. G. Ahunbay, J. Lee, Ş. B. Tantekin-Ersolmaz, Y. Chen, MXene materials for designing advanced separation membranes, Adv. Mater., 32 (2020) 1906697. https://doi.org/10.1002/adma.201906697

[34] N. Nasrollahi, L. Ghalamchi, V. Vatanpour, and A. Khataee, Photocatalytic-membrane technology: a critical review for membrane fouling mitigation, J. Ind. Eng. Chem., 93 (2021) 101–116. https://doi.org/10.1016/j.jiec.2020.09.031

[35] A. Khan, T. A. Sherazi, Y. Khan, S. Li, S. Ali Raza Naqvi, Z. Cui, Fabrication and characterization of polysulfone/modified nanocarbon black composite antifouling ultrafiltration membranes, J. Membr. Sci., 554 (2018) 71–82. https://doi.org/10.1016/j.memsci.2018.02.063

[36] M. Ghidiu, M. R. Lukatskaya, M.-Q. Zhao, Y. Gogotsi, M. W. Barsoum, Conductive two-dimensional titanium carbide 'clay' with high volumetric capacitance, Nature, 516 (2014) 78-81. https://doi.org/10.1038/nature13970

[37] R. P. Pandey, P. A. Rasheed, T. Gomez, R. S. Azam, K. A. Mahmoud, A fouling-resistant mixed-matrix nanofiltration membrane based on covalently cross-linked Ti_3C_2TX (MXene)/cellulose acetate, J. Membr. Sci., 607 (2020) 118139. https://doi.org/10.1016/j.memsci.2020.118139

[38] Q. Xue, K. Zhang, MXene nanocomposite nanofiltration membrane for low carbon and long-lasting desalination, J. Membr. Sci., 640 (2021) 119808. https://doi.org/10.1016/j.memsci.2021.119808

[39] D. Xu, X. Zhu, X. Luo, Y. Guo, Y. Liu, L. Yang, X. Tang, G. Li, H. Liang, MXene Nanosheet Templated Nanofiltration Membranes toward Ultrahigh Water Transport, Environ. Sci. Technol., 55 (2021) 1270–1278. https://doi.org/10.1021/acs.est.0c06835

[40] X. Zhao, Y. Che, Y. Mo, W.Huang , C. Wang, Fabrication of PEI modified GO/MXene composite membrane and its application in removing metal cations from water, J. Membr. Sci., 640 (2021) 119847. https://doi.org/10.1016/j.memsci.2021.119847

[41] V. R. Pereira, A. M. Isloor, U. K. Bhat, A. F. Ismail, A. Obaid, and H. K. Fun, Preparation and performance studies of polysulfone-sulfated nano-titania ($S\text{-}TiO_2$) nanofiltration membranes for dye removal, RSC Adv., 5 (2015). https://doi.org/10.1039/c5ra07994b

[42] A. Khan, T. A. Sherazi, Y. Khan, S. Li, S. Ali Raza Naqvi, Z. Cui, Fabrication and characterization of polysulfone/modified nanocarbon black composite antifouling ultrafiltration membranes, J. Membr. Sci., 554 (2018) 71–82. https://doi.org/10.1016/j.memsci.2018.02.063

[43] L. Feng, Z. Zhang, Z. Mai, Y. Ma, B. Liu, L. Jiang, D. Zhu, A Super-Hydrophobic and Super-Oleophilic Coating Mesh Film for the Separation of Oil and Water, Angew. Chem., 116 (2004) 2046–2048. https://doi.org/10.1002/ange.200353381

[44] D. Sun, M. Q. Liu, J. H. Guo, J. Y. Zhang, B. B. Li, D. Y. Li, Preparation and characterization of PDMS-PVDF hydrophobic microporous membrane for membrane distillation, Desalination, 370 (2015) 63–71. https://doi.org/10.1016/j.desal.2015.05.017

[45] J. Haberkamp, M. Ernst, G. Makdissy, P. M. Huck, M. Jekel, Protein fouling of ultrafiltration membranes - Investigation of several factors relevant for tertiary wastewater treatment, J. Environ. Eng. Sci., 7 (2008) 651–660. https://doi.org/10.1139/S08-038

[46] S. Gul, Z. A. Rehan, S. A. Khan, K. Akhtar, M. A. Khan , M. I. Khan , M. I. Rashid , A. M. Asiri , S. B. Khan, Antibacterial PES-CA-Ag_2O nanocomposite supported Cu nanoparticles membrane toward ultrafiltration, BSA rejection and reduction of nitrophenol, J. Mol. Liq., 230 (2017) 616–624.